ANL/EBR-016

SUITABILITY OF SOME COMPONENTS OF THE EBR-II SODIUM SYSTEMS FOR OPERATION AT 62.5 MWt

by

N. Bulut

EBR-II Project
Argonne National Laboratory
Argonne, Illinois - Idaho Falls, Idaho

July 1970

Work performed under the auspices of the U. S. Atomic Energy Commission

TABLE OF CONTENTS

LIST OF FIGURES

LIST OF TABLES

SUITABILITY OF SOME COMPONENTS OF THE EBR-II SODIUM SYSTEMS FOR OPERATION AT 62.5 MWt

by

N. Bulut

ABSTRACT

In preparing for operation of EBR-II at 62.5 MWt, the stress criteria that guided the original design of the major components of the EBR-II sodium systems were re-evaluated and, in some cases, re-analyzed. The philosophy behind the codes on which the original design was based had changed since that design was completed. The re-evaluation and re-analysis of stresses due to static, thermal steady-state, and thermal transient loadings show that the major components have sufficient structural integrity for 62.5-MWt operating conditions.

I. INTRODUCTION

The reactor and the primary, secondary, and auxiliary systems of the EBR-II facility were designed for operation at a reactor power of 62.5 MWt. Until September 1969, however, the reactor had not been operated above 50 MWt. During run 38A (September 14 to 28, 1969), the power level of the reactor was increased, in steps, from 50 to 56 to 62.5 MWt. During this test run, all reactor and plant components performed satisfactorily. After run 38A, the power level was returned to 50 MWt, where it is being held for an interim period to permit modification of existing experimental subassemblies and design of future experiments for continuous 62.5-MWt operation.

Before run 38A, the original design bases for various components of the EBR-II facility were reviewed and re-evaluated; where necessary, the design was re-analyzed. This effort was warranted because some of the philosophy behind the "ASME Boiler and Pressure Vessel Code"[1], on which the designs of some of the components were based, has changed within the last 10 years. For instance, the original analysis and design for EBR-II were guided by the "maximum allowable stress" (S_a) values of the 1959 edition of

Section VIII (Unfired Pressure Vessels) of the Code. Division 2 of the 1968 edition of the same section (VIII), as well as of Section III (Nuclear Vessels), recommend the use of "design stress intensity" (S_m) values, which are higher than the S_a values used for the original design. Furthermore, the 1968 editions of Sections III and VIII (Division 2) permit a more liberal method (hopper diagram) of combining various categories of calculated stresses for comparison with the S_m values.

This report discusses the results of evaluation and, in some instances, re-analysis of the design of the following components and systems:

Reactor Vessel
Intermediate Heat Exchanger (IHX)
Primary-sodium Pumps
Primary-sodium Piping
Secondary-sodium Piping
Evaporators
Superheaters

II. REACTOR VESSEL

The design of the EBR-II reactor vessel (see Fig. 1) was analyzed for static and thermal stresses by the Franklin Institute, as part of the design effort in 1960. The final report of the analysis concluded that the stresses produced by steady-state and transient operating conditions were not excessive.

The stress analysis was based on three different loadings:

(1) steady-state operation at 62.5 MWt;

(2) reactor scram from full power while all primary-sodium pumps remain in operation; and

(3) reactor scram from full power after cessation of all primary-sodium-pumping power.

The boundary conditions assumed for the design of the reactor vessel are believed to be conservative. For instance:

(1) The bulk temperature of the primary sodium at the reactor-vessel outlet was assumed to be 900°F. This temperature was measured as 883°F during the 62.5-MWt operation of run 38A.[2]

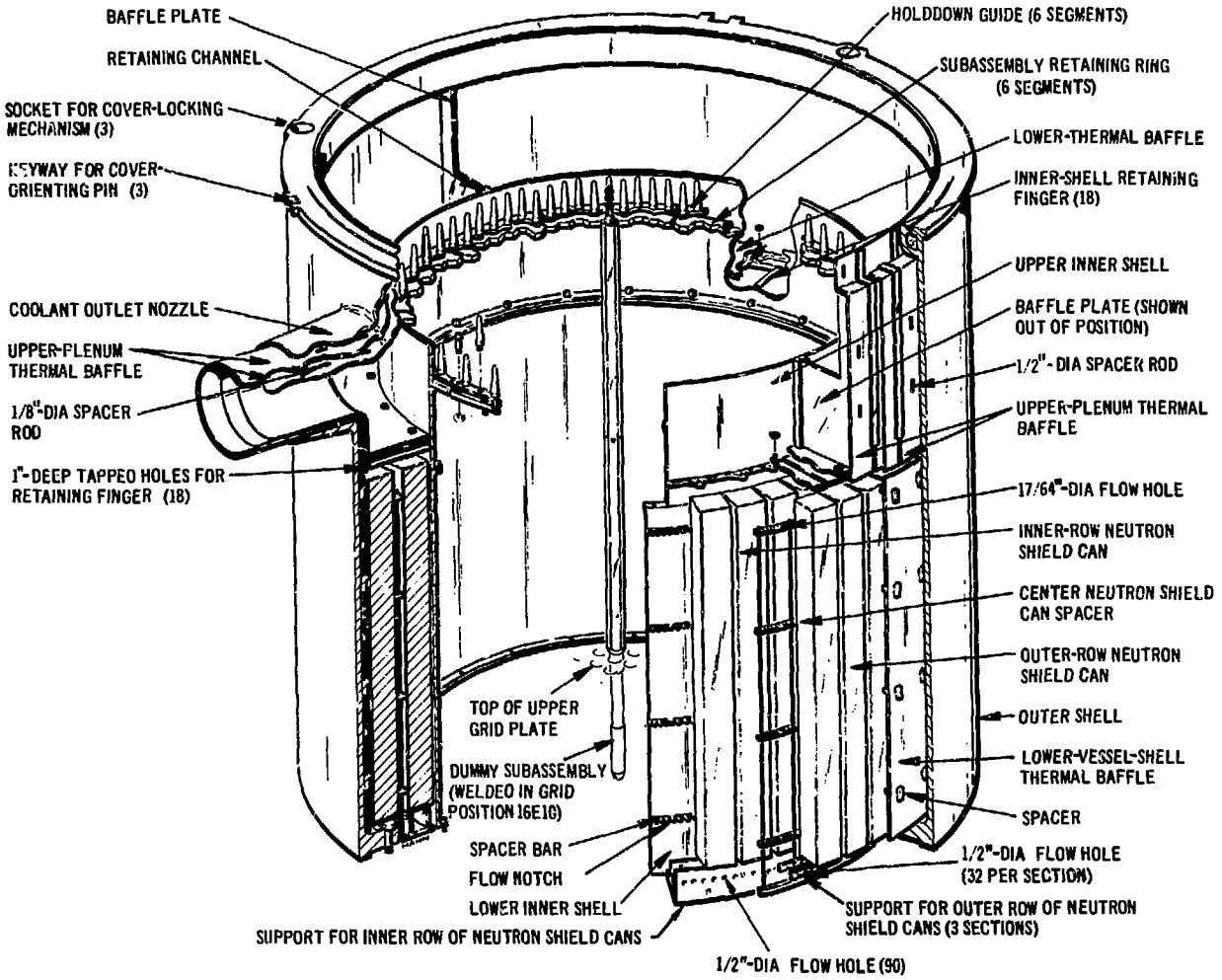

Fig. 1. EBR-II Reactor Vessel

(2) Figure A-27 of the "EBR-II Hazard Summary Report"[3] (on which the original design was based) shows time-dependent distribution of the temperature of the primary sodium at various points in the reactor vessel during a scram following cessation of all primary-sodium-pumping power. This figure was based on the flow-decay characteristics of the dc electromagnetic pumps that were contemplated as the main primary-sodium pumps in the original EBR-II design. The actual main primary-sodium pumps are of the mechanical, centrifugal type. Because of the momentum of the impeller, drive shaft, and motor of this type of pump, the primary-sodium flow decays much slower than with a dc electromagnetic pump after cessation of pumping power. Thus, as shown in Fig. F-3 of the "Addendum to the Hazard Summary Report,"[4] the average sodium temperatures at core-subassembly outlets and at plenum inlet and outlet have lower maxima than used for the original design.

(3) Design of the reactor vessel was based on a pressure drop of 20 psi in the primary sodium between the outlet plenum and the reactor tank. This drop is actually about 12 psi at full flow of the primary sodium.

(4) The stress analysis assumed that natural convection would provide a flow of bulk sodium (at 700°F) along the outer neutron-shield liner that would be sufficient to maintain a sodium temperature of 700°F at the lower half of the outlet nozzle for the primary sodium. Because of this assumption, unnecessarily high ΔT values were used in calculating the thermal stresses in the primary-sodium outlet nozzle. The actual construction of the reactor vessel incorporates a shelf (see Fig. 2) designed to reduce natural convection flow of the 700°F sodium along the outer neutron-shield liner. Therefore, for both steady-state and transient conditions, the actual temperature differential and the resultant thermal stresses in the outlet nozzle are considerably lower than those assumed for the analysis.

(5) The values for "maximum allowable stress" (S_a) used in the analysis were taken from the 1959 edition of Section VIII (Unfired Pressure Vessels) of the Ref.-1 code (Material SA-240, Type 304 high-alloy steel, in Table UHA-23). Table UHA-23 in the 1968 edition of Division 1 (Pressure Vessels) of Section VIII lists higher values for "maximum allowable stress" (S_a) for the same material. Furthermore, Table AHA-1 in the 1968 edition of Division 2 (Alternative Rules for Pressure Vessels) of Section VIII and Table N-421 of the 1968 Section III (Nuclear Vessels) permit the use of "design stress

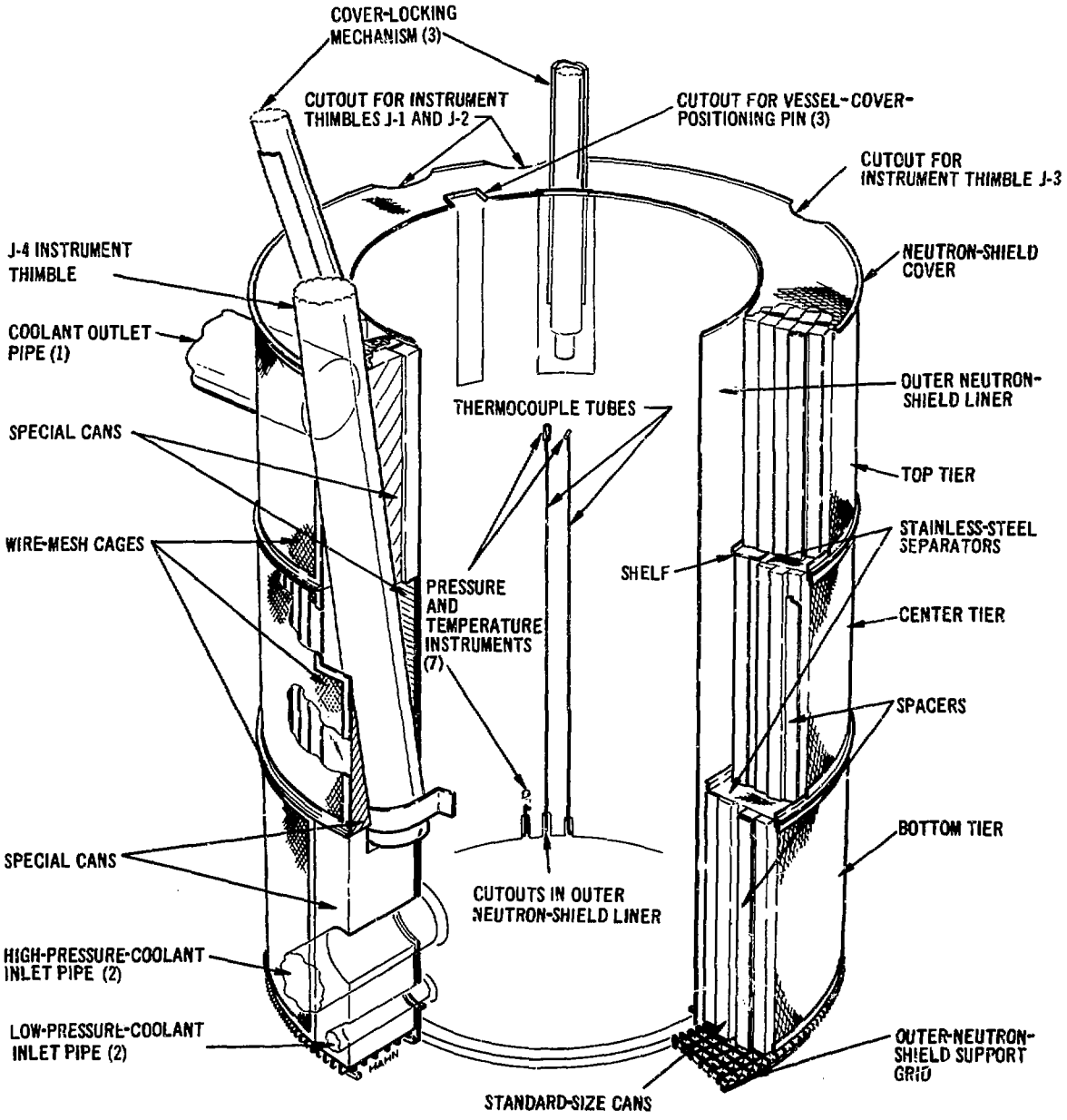

Fig. 2. Arrangement of Outer Neutron Shield around EBR-II Reactor-vessel Assembly

intensity" (S_m) values and recommend a more liberal method (hopper diagram) of combining various categories of actual stress for comparison with the tabulated S_m values. Table I of this report compares the values for the "maximum allowable stress" (S_a) and "design stress intensity" (S_m) cited above and also lists the yield strength (S_y) for the SA-240 (Type 304 high-alloy) material.

III. INTERMEDIATE HEAT EXCHANGER

During the design of the EBR-II facility, the Franklin Institute also performed preliminary and final stress analyses of the intermediate heat exchanger (IHX). Stresses due to static loading and to thermal steady-state and thermal transient loadings were investigated and were reported in 1960. The final analysis was complete and does not contain any major simplifying assumptions. Stresses were calculated for four different loadings (see Figs. 3 and 4):

(1) static loading with a secondary-sodium pressure of 150 psig and a reaction force of 1271 lb on the 14-in.-OD sleeve* around the secondary-sodium inlet pipe;

(2) steady-state thermal loading with the mean temperature of the center shell 20.9°F higher than that of the tubes;

(3) transient thermal loading (T1) for a reactor scram that causes the mean temperature of the center shell to be 60°F higher than that of the tubes; and

(4) transient thermal loading (T2) for a failure of the secondary-sodium pump that causes the mean temperature of the center shell to be 60°F lower than that of the tubes and a 200°F rise in temperature at the outer edge of the lower tubesheet.

Our evaluation of the analysis for each of these loadings follows.

A. Static Loading

The report on the final analysis revealed that, for static loading, the peak stress at a discontinuity exceeds the yield strength of the material at only one location: in the lower head of the IHX, where the wall of the inner shell is joined to the ring body (Point 7 of Body 5 in Fig. 4).

*This sleeve is from here on referred to as the center shell of the IHX.

TABLE I. Temperature vs Stress Characteristics of SA-240 (Type 304 High-alloy Steel) Given in ASME Code

	Section VIII				Section III	
	1959	1968			1968	
	Table UHA-23	Division 1, Table UHA-23		Division 2, Table AHA-1	Table N-421	Table N-424
Temp, °F	Maximum Allowable Stress (S_a), psi	Maximum Allowable Stress (S_a),[a] psi	Maximum Allowable Stress (S_a), psi	Design Stress Intensity (S_m), psi	Design Stress Intensity (S_m), psi	Yield Strength (S_y), psi
100	18,750	18,750	18,750	20,000	Same	30,000
200	16,650	16,550	16,000	20,000	as	25,600
300	15,000	15,500	13,750	19,800	in	22,000
400	13,650	14,950	12,250	17,600	column	19,600
500	12,500	14,550	11,400	16,400	at	18,200
600	11,600	14,350	10,800	15,600	left	17,300
700	10,800	14,200	10,500	15,100		16,800
800	10,000	14,000	10,250	14,800		16,400
900	9,400	13,600	10,000	14,400[b]		16,000
1000	8,800	12,500	9,450	13,600[b]		15,150

[a] These values are not recommended for design of flanges or piping.

[b] Extrapolated as $0.9S_y$.

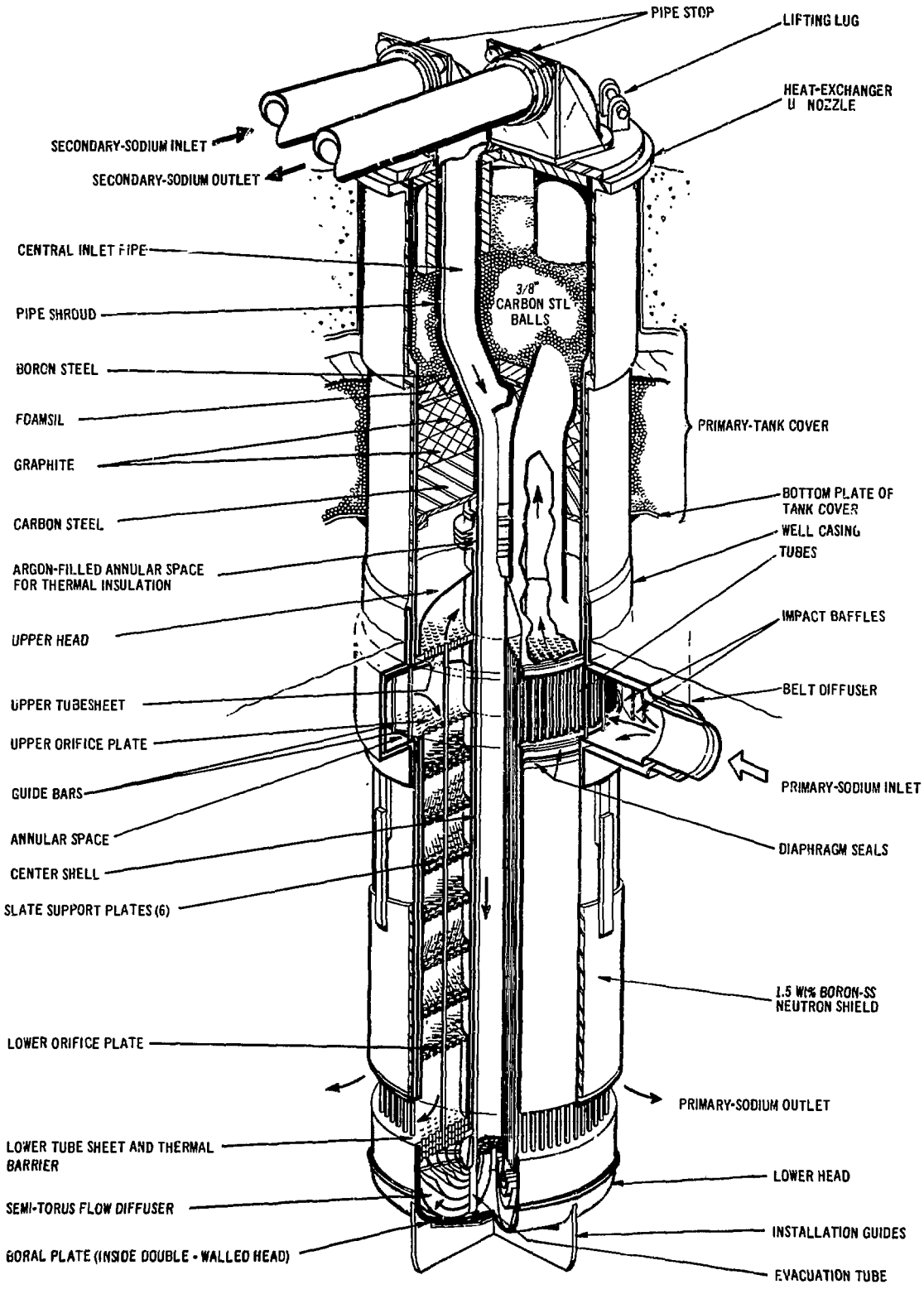

Fig. 3. EBR-II Intermediate Heat Exchanger (IHX)

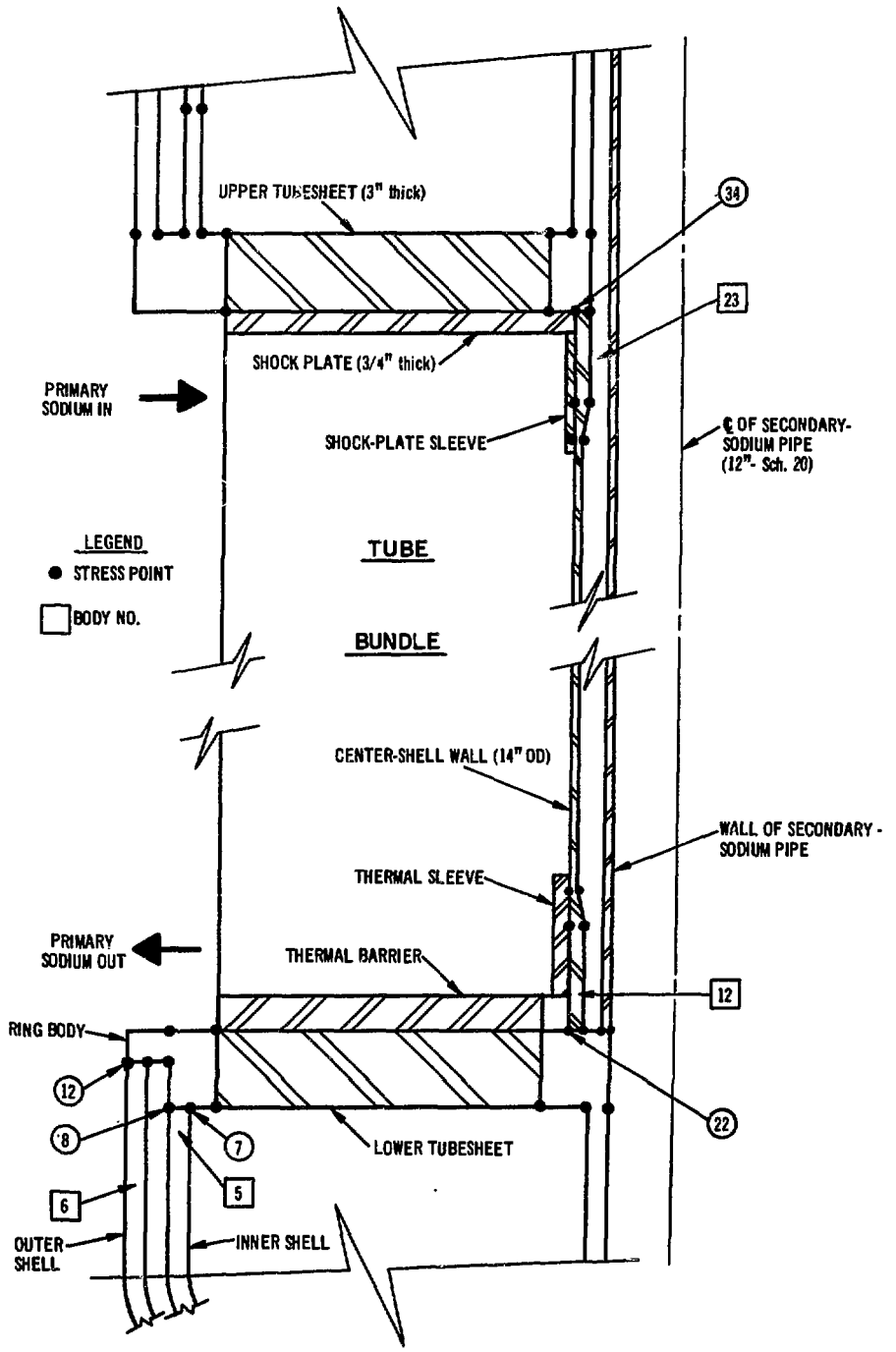

Fig. 4. Location of Points at which Stresses in IHX Were Calculated (only those points discussed in text are numbered)

According to the report, however, local plastic strain would take place at this joint during hydrostatic testing at the specified pressure of 340 psig. It was predicted that this first plastic cycle would produce sufficient cold spring for the joint to remain in the elastic range under 62.5-MWt operating conditions. Table II shows the axial stress, hoop stress, and maximum stress intensity under static loading at Points 7 and 8 of Body 5, the two locations of highest static (primary) stress in the IHX.

TABLE II. Maximum Stress (kpsi) in IHX under Static Loading

Body No.	5	5
Point No.	7	8
Axial Stress (σ_ℓ)	21.5	-17.0
Hoop Stress (σ_t)	- 5.5	- 6.1
Maximum Stress Intensity (σ_R)	27.0	17.0

B. Thermal Loadings

1. Steady State

Examination of steady-state thermal loadings revealed only one location of relatively high thermal stress: the outside surface of the circumferential weld joining the lower head of the IHX to the ring body (Point 12 in Fig. 4). At this point, the axial and hoop stresses due to steady-state thermal loading are about -18,600 and -13,130 psi, respectively. The axial stress (due to static loading) is about -5000 psi, and the hoop stress due to static loading is negligible. The principal stresses are determined from the equations

$$\sigma_1 = \sigma_{\ell 1} + \sigma_{\ell 2}, \tag{1}$$

$$\sigma_2 = \sigma_{t1} + \sigma_{t2}, \text{ and} \tag{2}$$

$$\sigma_3 = \sigma_{r1} + \sigma_{r2}, \tag{3}$$

where σ_1, σ_2, and σ_3 are the axial, hoop, and radial principal stresses, respectively; $\sigma_{\ell 1}$, σ_{t1}, and σ_{r1} are the axial, hoop, and radial stresses due to static loading, respectively; and $\sigma_{\ell 2}$, σ_{t2}, and σ_{r2} are the axial,

hoop, and radial stresses due to steady-state thermal loading, respectively. Calculations made by Franklin Institute during design of the IHX showed that σ_3 is equal to zero.

Substituting the stress values for Point 12 in Eqs. 1 and 2 gives σ_1 = -23,600 psi and σ_2 = -13,130 psi.

The maximum value (S_R) of the "equivalent intensity of combined stress" or, more briefly, "stress intensity" is the largest of the algebraic differences between the three principal stresses. These differences are: σ_{12} = -10,470 psi; σ_{23} = -13,130 psi; and σ_{31} = 23,600 psi. Therefore, $S_R = \sigma_{31}$ = 23,600 psi.

According to the 1968 editions of the ASME Code, however, stresses combined by hopper diagram may be three times the value of S_m at any given temperature. The temperature at Point 12 will not exceed 700°F. From Table I, S_m at 700°F is 15,100 psi. Three times this value (=45,300 psi) is much greater than the calculated value of 23,600 psi for S_R.

2. Transient from Reactor Scram (T1)

The analysis showed that the highest stress due to a reactor-scram transient (T1) occurs at a circumferential weld where the center shell is welded to the upper tubesheet (Point 34 in Fig. 4). Table III lists the stresses at this point under static loading and thermal-transient (T1) loading.

TABLE III. Maximum Stress (kpsi) in IHX during Thermal Transient due to Reactor Scram (T1)

Body No.	23
Point No.	34
Static Loading	
Axial Stress ($\sigma_{\ell 1}$)	- 4.2
Hoop Stress (σ_{t1})	- 1.9
Transient Loading	
Axial Stress ($\sigma_{\ell 2}$)	-28.0
Hoop Stress (σ_{t2})	-13.6

The principal stresses are determined as follows:

$$\sigma_1 = \sigma_{\ell 1} + \sigma_{\ell 2} = -4{,}220 - 28{,}040 = -32{,}260 \text{ psi}$$
$$\sigma_2 = \sigma_{t1} + \sigma_{t2} = -1{,}920 - 13{,}620 = -15{,}540 \text{ psi}$$
$$\sigma_3 = 0$$

The maximum stress intensity (S_R) is 32,260 psi (σ_{31}= 32,260). It represents the combination (by hopper diagram) of "primary local membrane stress" (P_L), "primary bending stress" (P_b), and "secondary membrane plus bending stresses" (Q), and should be compared with 3 x S_m. Since the secondary membrane stress is due to a temperature transient at Point 34, the value of S_m at that point can be taken as the average of the S_m values given in Table I for the highest and lowest temperatures of the weld during the transient. The highest temperature would be approximately 883°F, and the lowest about 720°F (20 sec after the scram). Based on these values, the interpolated value of S_m (from Table I) is approximately 14,700 psi. Since S_R is smaller than 44,100 psi (= 3 x 14,700), it is within the allowable limits.

The Franklin Institute report on stress analysis did not include calculations showing the transient thermal stresses produced in the upper tubesheet itself and in the center shell of the IHX. Subsequent calculations (see Appendix A) based on some simplifying, but very conservative, assumptions in boundary conditions have shown that the magnitudes of these stresses are far from being large enough to produce failure. The 3/4-in.-thick shock plate under the tubesheet and the shock-plate sleeve around the center shell are sufficient thermal barriers to keep the actual ΔT across both the tubesheet and the center shell relatively small.

3. Transient from Failure of Secondary-sodium Pump (T2)

The highest stress resulting from failure of the secondary-sodium pump (thermal transient T2) occurs at the inside surface of the circumferential weld joining the lower head of the IHX to the ring body (inside surface of Point 12). The second highest stress during transient T2 occurs at the circumferential weld (Point 22) joining the center shell and the lower tubesheet. Stresses at both points are listed in Table IV.

TABLE IV. Maximum Stresses (kpsi) in IHX during Thermal Transient due to Failure of Secondary-sodium Pump (T2)

Body No.	6	12
Point No.	12 (inside)	22
Static Loading		
Axial Stress ($\sigma_{\ell 1}$)	5.01	5.53
Hoop Stress (σ_{t1})	2.99	- 4.08
Transient Loading		
Axial Stress ($\sigma_{\ell 2}$)	35.72	34.94
Hoop Stress (σ_{t2})	- 8.08	19.14
Principal Stresses		
Axial ($\sigma_1 = \sigma_{\ell 1} + \sigma_{\ell 2}$)	40.73	40.47
Hoop ($\sigma_2 = \sigma_{t1} + \sigma_{t2}$)	- 5.09	15.06
Radial ($\sigma_3 = 0$)	0	0
Maximum Stress Intensity (σ_R)	45.82 (σ_{12})	40.47 (σ_{31})

Since the maximum stress intensity (σ_R) at point 12 (inside) exceeds 3 x S_m (=44,100), the stress was evaluated in accordance with fatigue-failure criteria. Since σ_R (45,820 psi) is higher than the yield strength, the material is in the plastic range. Fatigue damage in the plastic region has been found to be a function of plastic strain. Therefore, σ_R should be compared with data from tests in which strain, rather than stress, is the controlled variable. Figure 5* gives the results of such strain-controlled fatigue tests. As a matter of convenience, the strain values (e_t) used in the tests are multiplied by the elastic modulus (E_t) to give a fictitious stress that, although not the actual stress applied, may be compared directly with stresses calculated on the assumption of elastic behavior. From this, it follows that when σ_R is considered as an alternating stress, its amplitude (S'_a) will be

$$S'_a = \frac{1}{2} e_t E_t = \frac{1}{2} \sigma_R \qquad (4)$$

$$= 45,820/2 = 22,910 \text{ psi.}$$

Figure 5 shows that about 40,000 stress cycles would be required to produce fatigue failure at 900°F and an S'_a value of 22,910 psi. A transient caused by failure of the secondary-sodium pump is not expected to occur more than 500 times during the anticipated life of the EBR-II facility. Therefore, failure from strain fatigue should not occur at Point 12 (inside).

C. IHX Well Casing

Temperature readings have verified that during steady-state operation, hot primary sodium is forced upward in the annulus between the IHX well casing (welded to the U nozzle) and the tube-bundle structure of the IHX (see Fig. 3). The upward thrust of hot (883°F) sodium in this annulus is believed to cause thermal gradients between the 1-in.-thick wall of the well casing and the 2-in.-thick bottom plate of the reactor-tank cover to which it is attached by a 3/4-in. circumferential fillet weld.

---

*From Fig. 2 of "Case 1331-4" of Ref. 1.

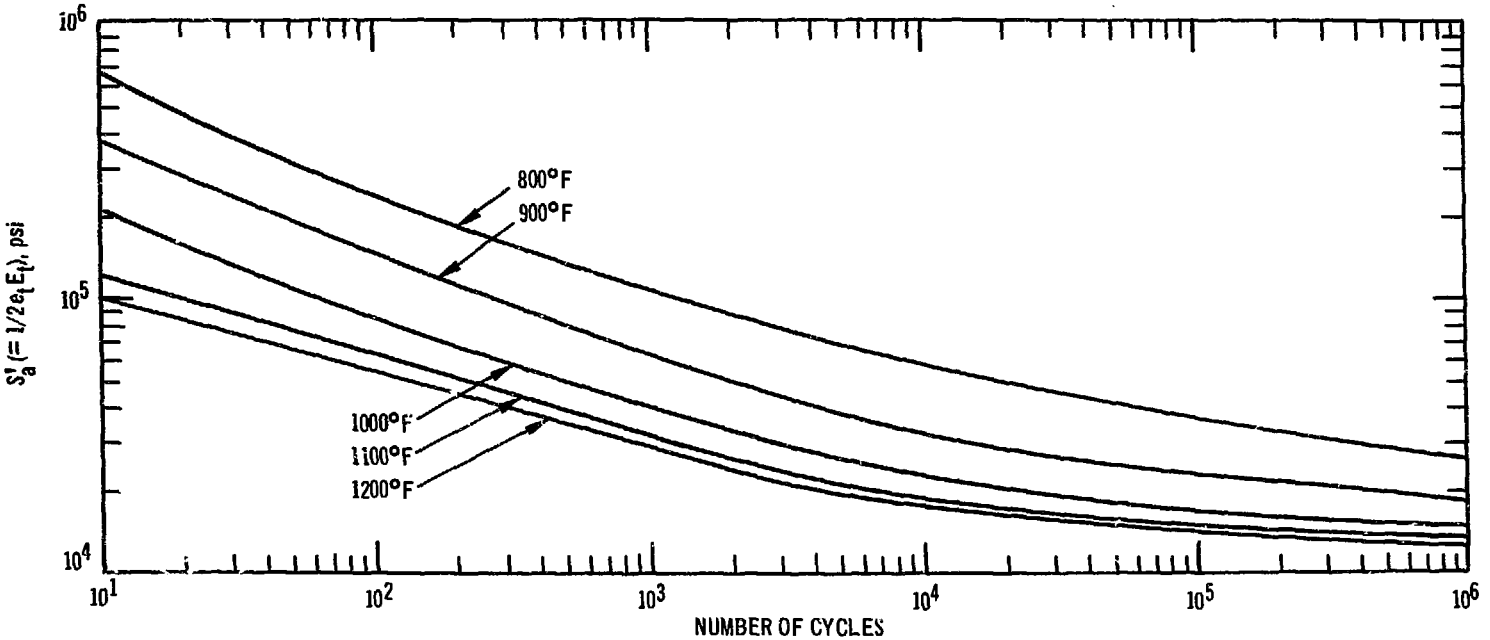

Fig. 5. Maximum Amplitude (S'_a) of Alternating Stress for High-alloy Steels and Nickel-Chrome-Iron Alloy up to 1200°F

The average temperature of the bottom plate of the reactor-tank cover is approximately 600°F, whereas the temperature of the well casing is assumed to reach 880°F*, which is almost the same as the temperature of the primary sodium at the inlet to the IHX. The thermal radial expansion of the U-nozzle opening in the 2-in. plate is negligible in comparison with the thermal radial expansion of the U nozzle itself. This difference in expansion causes stresses that produce local yielding in the shell wall of the well casing, the 2-in. bottom plate of the reactor-tank cover, and the fillet weld joining the two. The simple analysis reported in Appendix B showed that at least 2000 full-strain cycles would be required to produce fatigue failure in any member in this region. This figure is believed to be conservative because:

(1) The restraint that the 2-in. bottom plate of the reactor-tank cover provides to the expansion of the IHX well casing was not taken into account. The 3/4-in. fillet weld joining the well casing to the bottom plate was assumed to provide all the restraint required. Actually, the bottom plate will provide most of the total restraint; the fillet weld will be subjected to a relatively small fraction of the total load.

(2) Although the calculations in Appendix B were based on a 3/4-in. fillet weld, the actual size of the weld appears to be larger in the photographs taken during construction.

The above two considerations are conservatisms imposed by a desire to simplify the boundary conditions and the subsequent calculations. Other factors also contribute to the conservatism of the fatigue-failure analysis. These are inherent in the data provided by the ASME Code[1] and can be summarized as follows:

(1) Except for the brief period of 62.5-MWt operation in run 38A, EBR-II has never operated at a power level above 50 MWt. Since the temperature of the primary sodium at the IHX inlet is a function of the power level, the resultant thermal stresses at steady-state and transient conditions have been considerably lower than those calculated in Appendix B. A concentration of cycles of larger stress near the beginning of life of a component tends to accelerate failure, whereas if the smaller stresses are applied first and followed by progressively higher stresses, the "cumulative usage factor"

*The average of readings taken for this temperature during run 38A was approximately 868°F.

(UF)* can be increased to a value as high as 4 or 5.

(2) The design stress values for fatigue curves in the 1968 Section III of Ref. 1 were obtained from strain-controlled fatigue tests. The values were obtained from the best-fit curves by applying a factor of 2 on stress or a factor of 20 on cycles, whichever was more conservative at each point. These factors were intended to cover such effects as environment, size effect, and scatter of data.

D. IHX Performance Data

Table V compares predicted and measured values of IHX operating parameters at two power levels. The most significant difference between the predicted and measured values occurs in the secondary-sodium outlet temperature. As explained in Ref. 2, the predicted values of this temperature at 56- and 62.5-MWt operation were based on IHX performance at 50 MWt, when the coefficient of heat transfer was found to be 95% of the design coefficient.

TABLE V. Performance Data for the IHX

	Predicted	Measured	Predicted	Measured
Operating Power, MWt	56	56.5	62.5	62.3
Primary-sodium Flow Rate, lb/hr x 10^{-6}	3.82	3.86	3.82	3.81
Primary-sodium Inlet Temp, °F	700	700	700	700
Primary-sodium Outlet Temp, °F	864	864	883	883
Secondary-sodium Flow Rate, lb/hr x 10^{-6}	2.4	2.23	2.38	2.36
Secondary-sodium Inlet Temp, °F	584	588	585	586
Secondary-sodium Outlet Temp, °F	862	858	879	872
Secondary-sodium ΔP, psi	2.5	2.6	2.7	2.8

E. Channeling of Primary Sodium in the IHX

The IHX includes two features designed to achieve a balance of primary sodium: (1) a belt diffuser at the primary-sodium inlet; and (2) two orifice

---

*The cumulative effect of various stress cycles in a member is evaluated (in the 1968 Section III of Ref. 1) by means of a linear damage relationship in which it is assumed that if N_1 cycles would produce failure at a stress level S_1, then n_1 cycles at the same stress level would use up the fraction n_1/N_1 of the total life. Failure occurs when the cumulative usage factor (UF), which is the sum $n_1/N_1 + n_2/N_2 + n_3/N_3 + \ldots$, is equal to 1.0.

plates, one just below the primary-sodium inlet, and the other just above the primary-sodium outlet. Temperature readings taken at the lower orifice plate have indicated that the primary sodium is channeling at the inner and outer edges of the tube bundle. This channeling, near the center shell, causes the mean temperature of the center shell to be higher than the bulk temperature of the primary sodium (on which the design was based). Since the thermal stresses in the IHX are influenced by the difference between the mean temperatures of the center shell and the tubes, the resultant thermal stresses may actually be higher than those calculated during design.

The scope of this report does not include calculation of the thermal stresses caused by this channeling. Section VIII of the report, however, makes some recommendations on the subject.

IV. PRIMARY-SODIUM PUMPS

Since the flow of primary sodium and the temperature of the bulk sodium in the primary tank will be the same at 62.5 as at 50 MWt, the performance of the primary-sodium pumps should also be the same at the two power levels. In the early stages of EBR-II operation, both pumps were removed, modified, and reinstalled. Subsequent operation has been satisfactory and reliable.

V. PRIMARY-SODIUM PIPING

A thorough stress analysis by the Franklin Institute preceded design and fabrication of the primary-sodium piping loop between the reactor and the IHX. Relatively large stresses during a reactor-scram transient occur in portions of the loop where a gas insulation separates the inner and outer pipes. The largest thermal stress due to a reactor scram occurs in the region of the junction of the 14-in.-OD outer pipe and the electrode box section. All these stresses are within acceptable limits when compared with the design stress intensity values obtained by using Fig. N-414 (hopper diagram) of the 1968 Section III of Ref. 1.*

*Figure N-414 is equivalent to Table F-104 in the draft issue of Nuclear Power Piping, USAS B31.7, The American Society of Mechanical Engineers (February 1968).

VI. SECONDARY-SODIUM PIPING

A complete stress analysis of the secondary-sodium piping system was performed by Blaw-Knox Company in 1958. The resultant stresses were found to be well within the limits allowed in Fig. N-414 of the 1968 Section III of Ref. 1.*

VII. STEAM GENERATORS

A. Design Features

The EBR-II steam-generating train comprises two superheaters and eight evaporators, interconnecting piping, and a steam drum. The secondary sodium flows through the shell side of the two superheaters, which are connected in parallel, and then passes through the shell side of the eight evaporators, which also are connected in parallel (see Fig. 6). All 10 units are identical in construction except that the flow area of each superheater tube is reduced by a "core tube" (see Figs. 7 and 8). Each unit is a single-pass, shell-and-tube heat exchanger with a bundle of bonded duplex tubes. About 4 ft of each tube at the sodium-inlet end has an additional shield (thermal baffle tubes) to protect the duplex tubes from excessive thermal stresses resulting from steady-state and transient operating conditions. The sodium tubesheets are also protected by thermal baffles against thermal shock. Table VI shows some design parameters of the steam generators.

B. Design of Superheater Tubes

All 10 steam generators now in service in the EBR-II facility were originally designed as evaporators. The two that were modified to serve as superheaters are subject to temperatures of secondary sodium higher than those expected for the evaporators.

Calculations were made to verify the adequacy of the tubes for use in the superheaters. The calculations were based on the assumption that the

---

*Figure N-414 is equivalent to Table F-104 in the draft issue of Nuclear Power Piping, USAS B31.7, The American Society of Mechanical Engineers (February 1968).

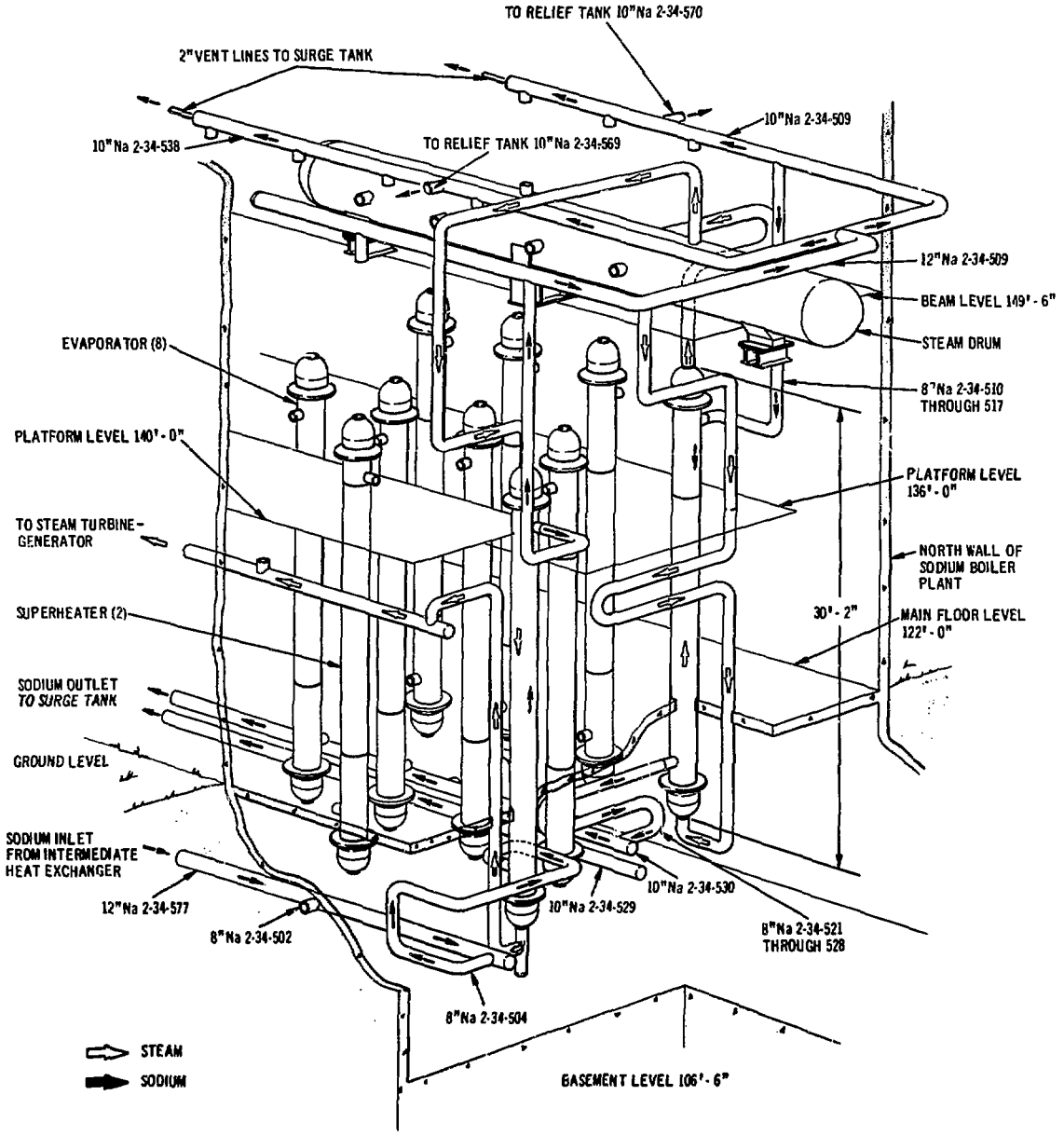

Fig. 6. EBR-II Steam-generating System

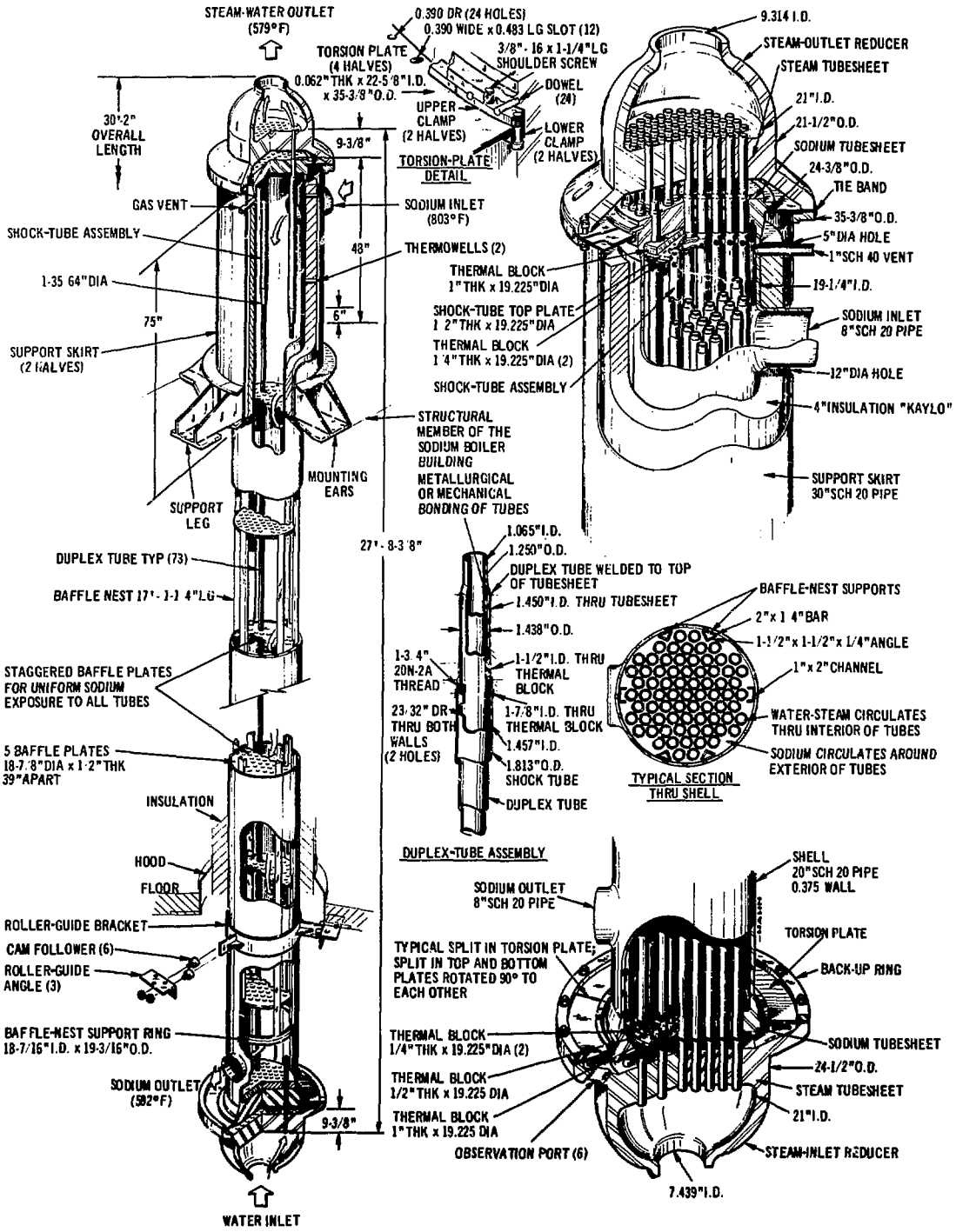

Fig. 7. EBR-II Evaporator Assembly

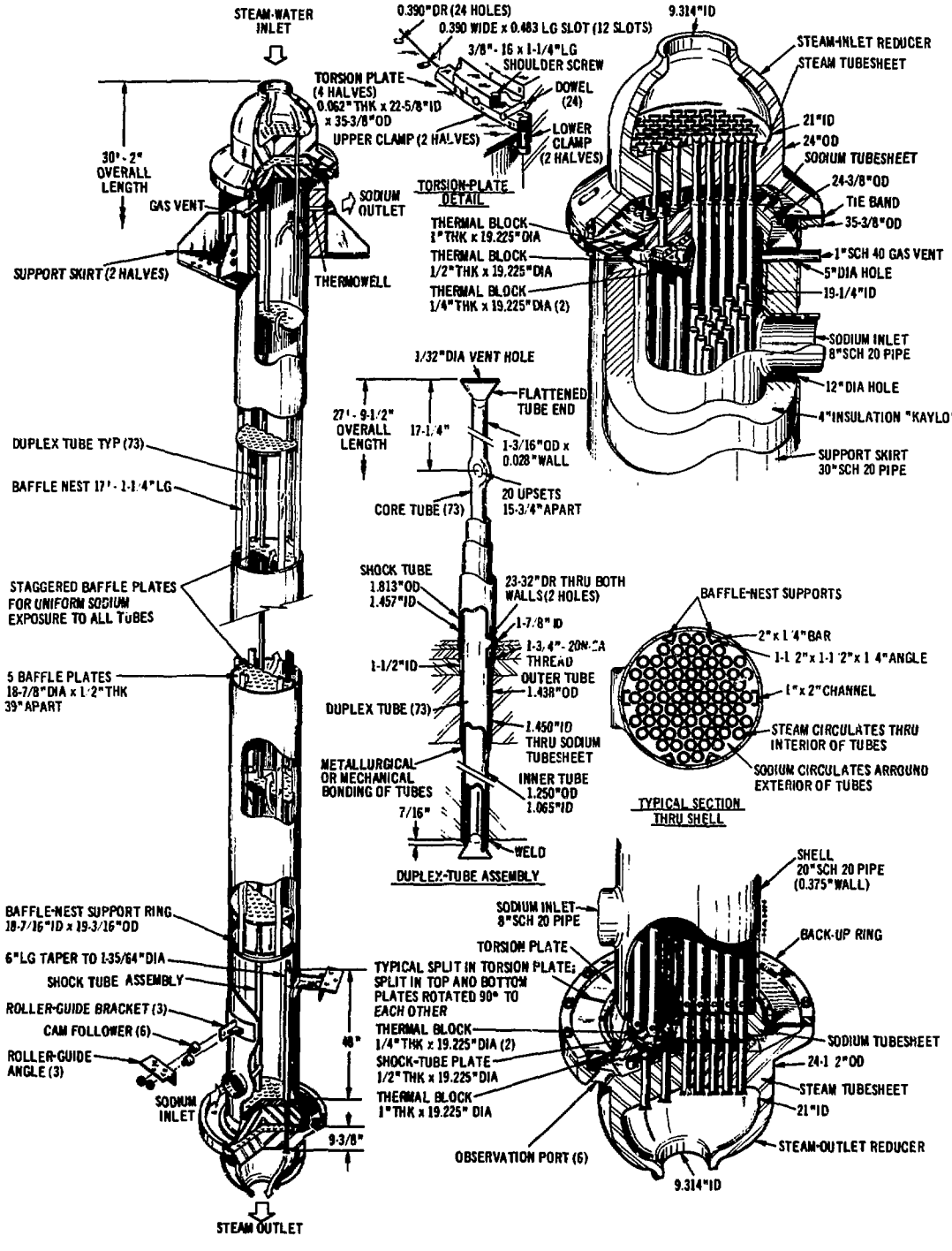

Fig. 8. EBR-II Superheater Assembly

TABLE VI. Design Parameters of EBR-II Steam Generators

Materials	
Shell	SA-387, Gr. D
Tubesheets and heads	SA-182, Gr. F22
Duplex tubes	SA-213, Gr. T22
Shell (Sodium) Side	
Design pressure, psig	150
Design temperature, °F	1000
Pneumatic test pressure, psig	365
Tube (Water or Steam) Side	
Design pressure, psig	1500
Design temperature (evaporators), °F	800
Design temperature (superheaters), °F	900
Hydrostatic test pressure (evaporators), psig	2250
Hydrostatic test pressure (superheaters), psig	2900
Inner-tube dimensions	
OD, in.	1.25
Wall thickness, in.	0.0925
Outer-tube dimensions	
OD, in.	1.43
Wall thickness, in.	0.0940

inner tube is the only pressure-carrying member of the duplex-tube structure. Allowable stress, internal pressure, and wall thickness of the tubes are related as follows:*

$$P = \frac{S_a \eta t}{R + 0.6t}, \qquad (5)$$

where P = internal pressure in psig,

S_a = maximum allowable stress in psi,

η = joint efficiency (assumed to be unity for seamless pipe),

t = thickness of tube wall in inches, and

R = inside radius of tube in inches.

Table VII shows values of S_a and the corresponding maximum safe values of P for the steam-generator tubes at various temperatures.

TABLE VII. Allowable Stresses and Pressures for EBR-II Steam-generator Tubes

Temperature, °F	Maximum Allowable Stress $(S_a)^a$, kpsi	Maximum Safe Internal Pressure (P), psig
800	15.0	2360
850	14.4	2265
900	13.1	2060
950	11.0	1730
1000	7.8	1227

[a]From Table UCS-23 of the 1959 Section VIII of Ref. 1.

The values for maximum safe internal pressure (P) in the table were calculated from Eq. 5, using the values for S_a given in the table, a joint efficiency (η) of 1.0, an inside tube radius (R) of 0.5325 in. (from Table VI), and a tube-wall thickness (t) of 0.0925 in. (also from Table VI). Table VII shows that for the superheater tubes, P is well above the design pressure of 1500 psig at the design temperature of 900°F.

Figures 9 and 10 respectively show the design and expected temperature profiles of the evaporator tubes at 62.5-MWt operation. Figures 11 and 12

*Paragraph UG-27(c) of the 1959 Section VIII of Ref. 1.

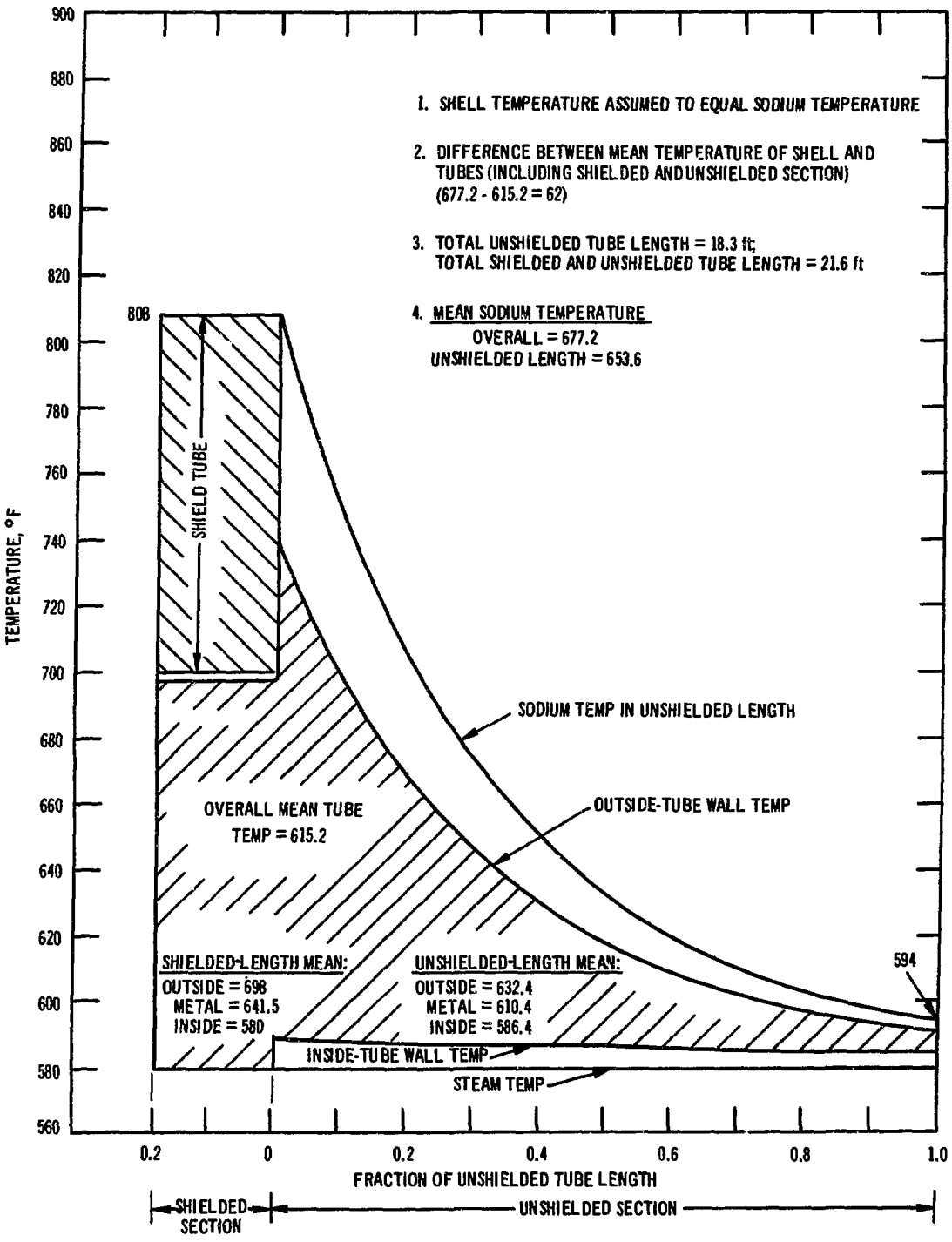

Fig. 9. Design Temperature Profiles of EBR-II Evaporators

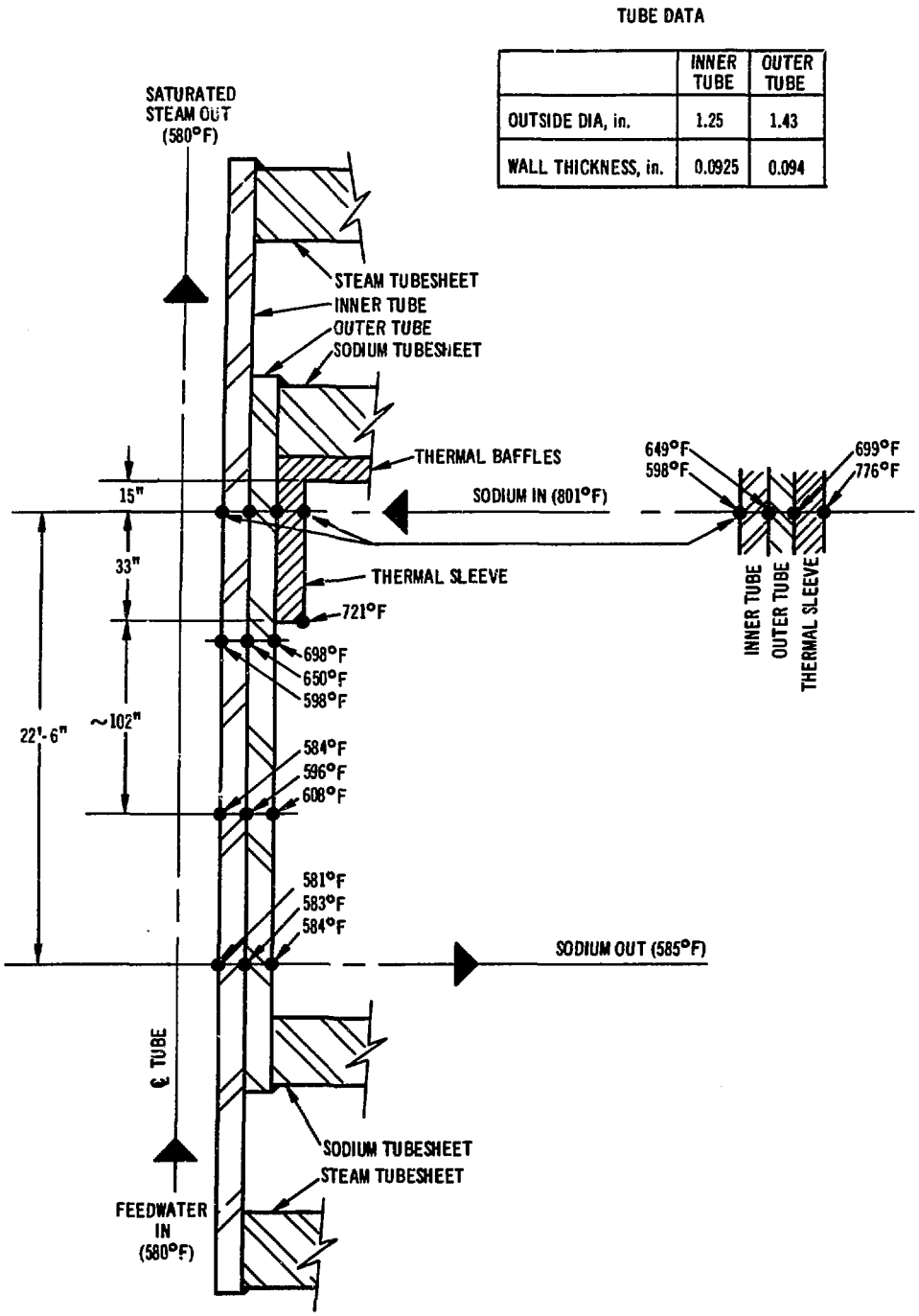

Fig. 10. Expected Temperature Profiles of EBR-II Evaporator Tubes at 62.5-MWt Operation

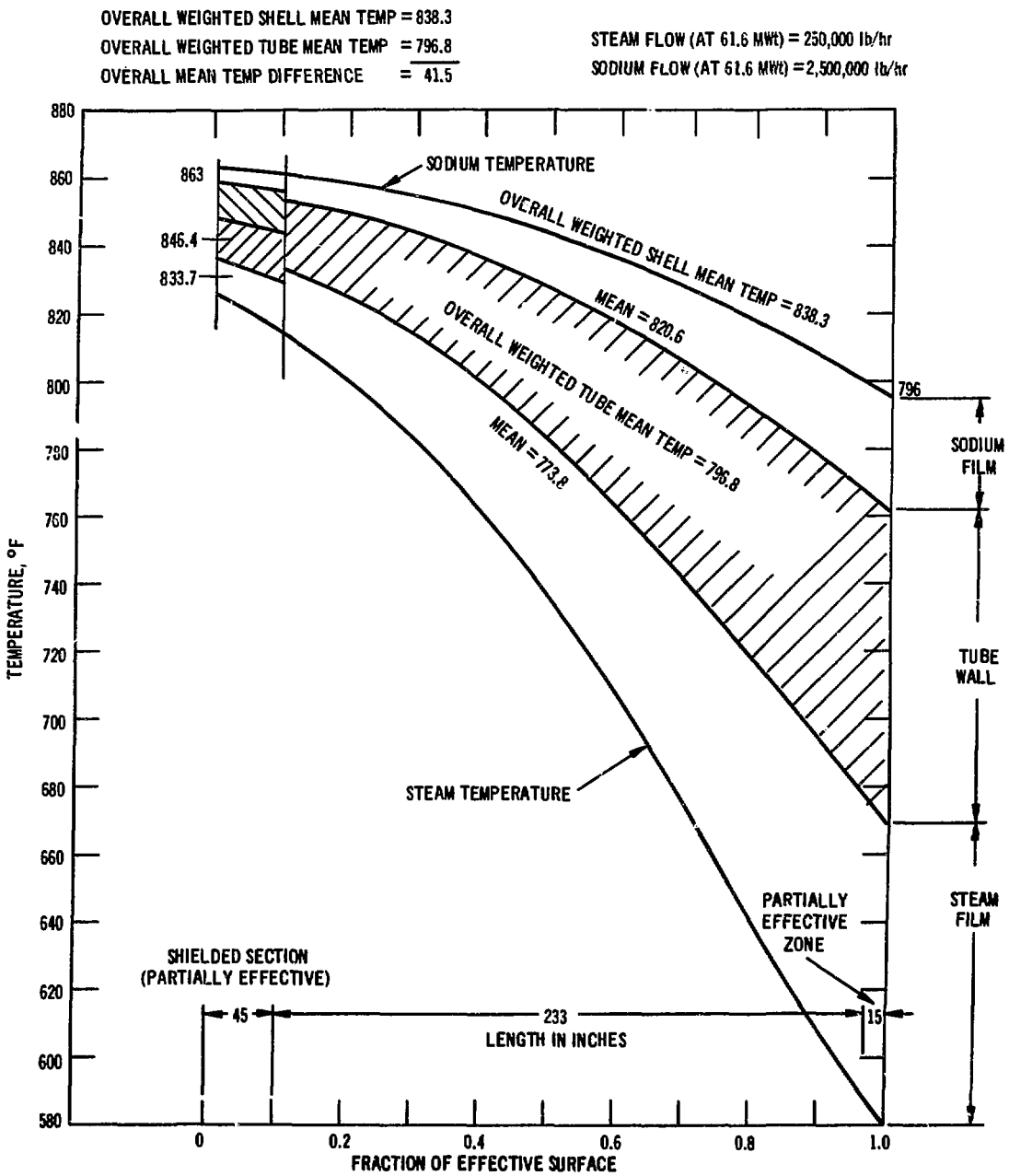

Fig. 11. Design Temperature Profiles of EBR-II Superheaters

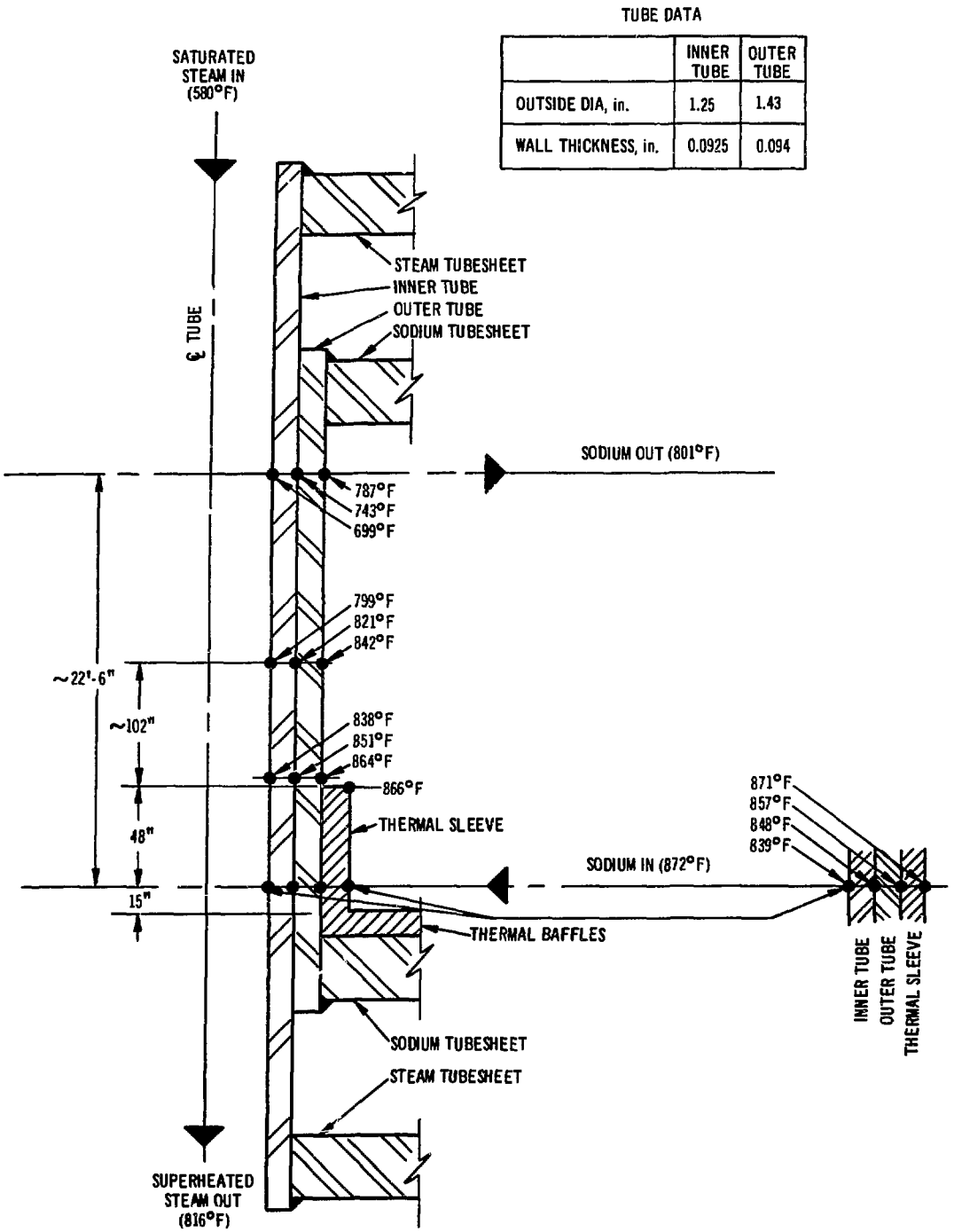

Fig. 12. Expected Temperature Profiles of EBR-II Superheater Tubes at 62.5-MWt Operation

respectively show the design and expected temperature profiles of the superheater tubes at 62.5-MWt operation. Figure 12 indicates that the maximum radial temperature difference (744-699°F = 44°F) in the inner tube of the superheater occurs at the secondary-sodium outlet end. The radial thermal stress (hoop stress) in the wall of the inner tube that results from this difference is calculated as follows:

$$\sigma_t = \frac{E\alpha\Delta T}{2(1-\nu)}, \qquad (6)$$

where

σ_t = hoop stress in psi,
E = modulus of elasticity (=24 x 10^6 psi at 743°F),
α = instantaneous coefficient of thermal expansion (=10.8 x 10^{-6} in./in.-°F at 743°F),
ΔT = radial temperature difference (=44°F), and
ν = Poisson's ratio (=0.3).

By substitution of the numerical values,

$$\sigma_t = \frac{(24 \times 10^6)\ (10.8 \times 10^{-6})\ 44}{2\ (1 - 0.3)}$$

$$= 8150 \text{ psi.}$$

The primary hoop stress due to internal pressure (1500 psi) at the same point is determined from Eq. 5 as 9540 psi.

Since the sum of these two stresses (17,690 psi) is less than three times the design stress intensity (S_m) of 15,600 psi* at the temperature of the point, the thickness of the wall of the inner tube is adequate.

In the above calculations, no credit is taken for the restraining effect of the outer tube on the inner tube. The actual primary hoop stress in the inner tube will be considerably smaller than the 9540 psi calculated, because the inner and outer tubes are bonded together to form a 0.1865-in. rather than a 0.0925-in. wall. The hoop stress calculated by Eq. 5, using this heavier wall thickness, is 5180 psi.

C. Stress Analysis

The design of the EBR-II evaporators was analyzed by the Franklin Institute in 1959. The loadings on which the stress analysis was based are:

*From Table N-421 of Section III, Ref. 1.

(1) pressure of feedwater and steam inside tubes = 1500 psig;

(2) shell-side pressure of secondary sodium = 50 psig; and

(3) difference between the mean temperatures of the shell and of the tubes = 62°F (this difference is the main cause of the thermal stresses).

The analysis did not reveal excessive stresses.

Some of the design, predicted, and measured parameters for the evaporators and the superheaters are shown in Tables VIII and IX, respectively. The predicted temperatures of the inlet secondary sodium and the inlet feedwater to the evaporators agree well with the measured values. Therefore, the actual difference between the mean temperatures of the shell and the tubes is considerably lower than the design value of 62°F. Consequently, the resultant thermal stresses are lower than design values. Use of the units as superheaters decreases this difference further (to 41.3°F).

D. Flow-induced Vibrations

The velocity of the secondary sodium through the superheaters is considerably higher than that through the evaporators. For this reason, the possible occurrence of flow-induced vibrations in the superheaters was of some concern before run 38A. During this run (in September 1969), the noise originating in each superheater was monitored. Accelerometers were mounted at three different locations on each superheater. Equipment was provided for: (1) direct listening, (2) recording on tape, and (3) a simple frequency-spectrum analysis. The character of the measured frequency spectrum (2-500 Hz) varied little as the power was increased from 20 to 62.5 MWt; however, there is considerable experimental uncertainty for these frequency data.

For other steam-generating equipment, personnel listened with a stethoscope for unusual noises or changes in sound originating in the equipment. Specific items monitored included steam piping, sodium piping, secondary-sodium EM pump, all evaporators, surge tank, steam drum, and feedwater piping. No unusual noise resulting from operating at 62.5 MWt was detected.

TABLE VIII. Operation and Design Parameters for EBR-II Evaporators

	Design[a]	Predicted[b]	Measured (Ref. 2)
Number of Units	8	8	8
Reactor Power, MWt	61.6	62.5	62.5
Shell Side (Sodium)			
Sodium flow rate, lb/hr x 10^{-6}	2.50	2.43	2.36
Sodium inlet temp, °F	808	801	800
Sodium outlet temp, °F	594	585	581
Overall shell mean temp, °F	677.2	647.8	---
Tube Side (Feedwater and Steam)			
Feedwater flow rate, lb/hr x 10^{-5}	2.70	2.75	2.65
Feedwater temp at steam-drum inlet, °F	580	550	560
Steam outlet temp, °F	580	580	580
Shielded Length of Tubes			
Outside mean temp, °F	698	647.7	---
Metal mean temp, °F	641.5	620.6	---
Inside mean temp, °F	580	590.3	---
Unshielded Length of Tubes			
Outside mean temp, °F	632.4	612.3	---
Metal mean temp, °F	610.4	600.2	---
Inside mean temp, °F	586.4	584.9	---
Overall Tube Mean Temp, °F	615.2	603.5	---
Difference between Mean Temperatures of Shell and Tubes, °F	62.0	44.3	---

[a] From Fig. 9.

[b] Projected values based on actual operation at power levels below 62.5 MWt (provided by C. C. Stone).

TABLE IX. Operation and Design Parameters for EBR-II Superheaters

	Design[a]	Predicted[b]	Measured (Ref. 2)
Number of Units	2	2	2
Reactor Power, MWt	61.6	62.5	62.5
Shell Side (Sodium)			
Sodium flow rate, lb/hr x 10^{-6}	2.50	2.43	2.36
Sodium inlet temp, °F	863	872	870
Sodium outlet temp, °F	796	801	800
Overall weighted shell mean temp, °F	838.3	844.3	---
Tube Side (Steam)			
Steam flow rate, lb/hr x 10^{-5}	2.50	2.55	2.50
Steam inlet temp, °F	580	580	580
Steam outlet temp, °F	834	816	819
Overall weighted tube mean temp, °F	796.8	803.0	---
Shielded Length of Tubes			
Outside mean temp, °F	857	841.7	---
Metal mean temp, °F	846.4	837.5	---
Inside mean temp, °F	833.7	828.8	---
Unshielded Length of Tubes			
Outside mean temp, °F	820.6	818.2	---
Inside mean temp, °F	773.6	770.7	---
Difference between Overall Weighted Mean Temperatures of Shell and Tubes, °F	41.5	41.3	---

[a] From Fig. 11.

[b] Projected values based on actual operation at power levels below 62.5 MWt (provided by C. C. Stone).

VIII. CONCLUSIONS AND RECOMMENDATIONS

The foregoing review leads to the conclusion that the components of the EBR-II sodium systems are suitable for operation at the original design power level of 62.5 MWt. Evaluation of performance capability and structural integrity revealed no deficiencies of serious concern. The highest stress in all components evaluated occurs in the fillet weld between the IHX well casing and the bottom plate of the reactor-tank cover. This high stress is caused by some of the hot primary sodium thrusting upward through the annulus between the well casing and the tube bundle. The stresses in this weld could be reduced by installing an additional seal in the annulus between the well casing and the tube bundle. This seal, similar to the one just below the primary-sodium inlet, would be placed just above that inlet and would reduce the temperature gradients near the weld.

It is also recommended that a separate and in-depth study be undertaken to analyze the thermal stresses in the IHX that result from channeling of the primary sodium (as described in Section III.E). In this study, thermal transients for which the stresses are to be analyzed should include those caused by: (1) scram of the reactor; (2) failure of the secondary pump; (3) failure of all primary pumps, including the auxiliary pump; and (4) ramp changes in the flow and temperature of the secondary sodium.

The completed review could not evaluate all possible effects of aging of the IHX during its years of operation. Structural weaknesses that might have developed during this aging could cause a failure and a resultant shutdown of the IHX and, thus, the reactor. The length of such a shutdown would be greatly reduced if a new tube bundle were on hand for immediate installation instead of repairing and reinstalling the existing one. Therefore, it is recommended that a spare tube bundle be procured so that it is ready to install if needed.

APPENDIX A

Transient Thermal Stress in the Upper Tubesheet of the Intermediate Heat Exchanger after Reactor Scram

During normal operation, the lower face of the 3/4-in.-thick shock plate under the upper tubesheet of the intermediate heat exchanger (IHX) is in contact with the primary sodium, whose temperature is 883°F. The upper face of the tubesheet is in contact with the secondary sodium, whose temperature is 872°F. Approximately 13 sec after a reactor scram, the temperature of the primary sodium at the inlet to the IHX, and thus at the lower face of the shock plate, will have fallen 150°F (according to Figure 55 of Ref. 4). The following calculations show the method used to determine the thermal stresses in the upper tubesheet that result from this transient.

The calculations incorporate the following simplifying assumptions:

1. The temperature at the lower face of the shock plate and the upper face of the tubesheet are the same;

2. the temperature drop of 150°F in the primary sodium occurs as a step change;

3. heat transfer from the secondary sodium in the tubes to the tubesheet is ignored; and

4. the assembly of the upper tubesheet and the shock plate is assumed to be a slab with an infinite surface area and a semi-infinite thickness.

The temperature at any point in the tubesheet is a function of position (distance from the lower face of the shock plate) and time, and is designated by $T(x,\theta)$. The temperature at the lower face of the shock plate is indicated by $T(0,\theta)$ and at a point "ℓ" ft from the surface by $T(\ell,\theta)$. Figure 13 shows the model used for the calculations.

In deriving the differential equation to describe the heat conduction in the slab, it is helpful to first write an energy-balance equation over the differential length (Δx) of the slab:

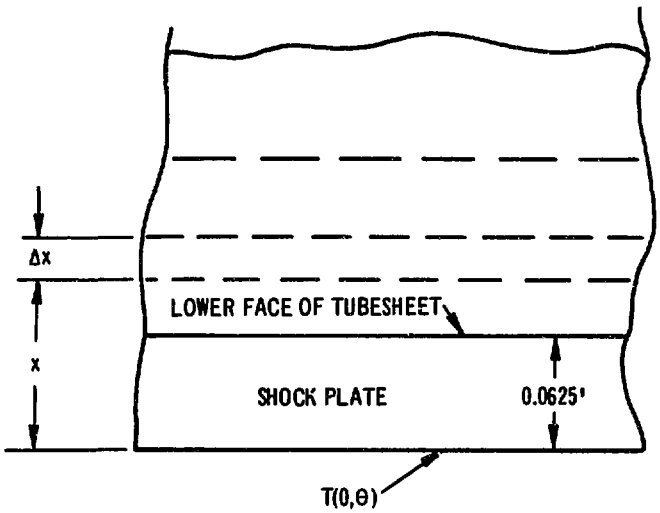

Fig. 13. Model for Calculating Thermal Stress in Intermediate Heat Exchanger after Reactor Scram

[Flow of heat by conduction from the lower face of slab to primary sodium] − [Flow of heat by conduction through slab to lower face] = [Rate of depletion of internal energy in a given volume of the slab

By applying Fourier's law of heat conduction ($q = -k \frac{\partial T}{\partial x}$) to our energy-balance equation, we obtain

$$-Ak \frac{\partial T}{\partial x}\Big|_{x + \Delta x} + Ak \frac{\partial T}{\partial x}\Big|_{x} = -\frac{\partial}{\partial \theta} [\rho CA\Delta x(T-T_r)], \tag{7}$$

where A = heat-transfer area, in ft^2;

k = thermal conductivity, in Btu/hr-ft-°F

(=11.5 for Type 304 stainless steel);

T = temperature, in °F;

x = distance from lower face of shock plate, in ft;

Δx = incremental thickness of slab, in ft;

θ = time after step change of 150°F at lower face of shock plate, in hr;

C = specific heat of metal, in Btu/°F-lb (=0.12 for Type 304 stainless steel);

ρ = density of metal, in lb/ft^3 (= 500 for Type 304 stainless steel); and

T_r = reference temperature used to evaluate internal energy, in °F.

By expanding the term $\frac{\partial T}{\partial x}\Big|_{x + \Delta x}$ according to the rule of Taylor series expansion, and taking the first two terms,

$$\Psi(x + \Delta x) = \Psi(x) + \frac{\partial}{\partial x}\Psi(x)\Delta x, \qquad (8)$$

where

$\Psi(x) = \frac{\partial T}{\partial x}$, we obtain

$$\frac{\partial T}{\partial x}\Big|_{x + \Delta x} = \frac{\partial T}{\partial x}\Big|_x + \frac{\partial}{\partial x} \cdot \frac{\partial T}{\partial x}\Delta x. \qquad (9)$$

By substituting this in Eq. 7 and simplifying, we obtain

$$-k\frac{\partial T}{\partial x}\Big|_x - k\frac{\partial}{\partial x} \cdot \frac{\partial T}{\partial x}\Delta x + k\frac{\partial T}{\partial x}\Big|_x = \frac{\partial}{\partial \theta} \cdot [\rho C \Delta x (T - T_r)],$$

which reduces to

$$-k\frac{\partial^2 T}{\partial x^2} = -\rho C \frac{\partial T}{\partial \theta},$$

and can be simplified to

$$K \frac{\partial^2 T}{\partial x^2} = \frac{\partial T}{\partial \theta} , \tag{10}$$

where K = thermal diffusivity, in ft^2/hr,

= $k/\rho C$.

Equation 10 is the fundamental equation describing conduction of heat in a solid. It can be solved by the method of Laplace transforms. Taking the Laplace transform of each term of Eq. 10 gives

$$K \int_0^\infty \frac{\partial^2}{\partial x^2} (x,\theta)\, e^{-s\theta} d\theta \int_0^\infty \frac{\partial T}{\partial \theta} (x,\theta)\, e^{-s\theta} d\theta. \tag{11}$$

By changing the order of integration and differentiation of the left side, we obtain

$$K \int_0^\infty \frac{\partial^2 T}{\partial x^2} (x,\theta)\, e^{-s\theta} d\theta = \frac{\partial^2}{\partial x^2} \int_0^\infty T(x,\theta)\, e^{-s\theta} d\theta = \frac{d^2 \bar{T}(x,s)}{dx^2} , \tag{12}$$

where $\bar{T}(x,s)$ is the Laplace transform of $T(x,\theta)$. The overbar indicates the Laplace transform of a function of two variables.

Application of the rule for Laplace transform of a derivative to the right side of Eq. 11 yields

$$\int_0^\infty \frac{\partial T}{\partial x} (x,\theta)\, e^{-s\theta} d\theta = s\bar{T}(x,s) - T(x,0), \tag{13}$$

where $T(x,0)$ is the initial temperature distribution in the tubesheet at time zero ($\theta = 0$).

Substituting the results of Eqs. 12 and 13 in Eq. 10 yields

$$K \frac{d^2\bar{T}(x,s)}{dx^2} = s\bar{T}(x,s) - T(x,0). \tag{14}$$

Since we are interested in deviation of the temperature from its value at $\theta = 0$, we shall assume the initial temperature to be zero $[\bar{T}(x,0) = 0]$. With this assumption, Eq. 14 can be simplified to

$$\frac{d^2\bar{T}(x,s)}{dx^2} - \frac{s}{K}\bar{T}(x,s) = 0. \tag{15}$$

This equation is a homogeneous linear differential equation, which has the solution

$$\bar{T}(x,s) = A_1 e^{-x\sqrt{s/K}} + A_2 e^{x\sqrt{s/K}}, \tag{16}$$

where A_1 and A_2 are arbitrary coefficients.

To keep $\bar{T}(x,s)$ finite as x approaches infinity, A_2 must equal zero. Therefore, Eq. 16 becomes

$$\bar{T}(x,s) = A_1 e^{-x\sqrt{s/K}}. \tag{17}$$

The transformed forcing function at $x = 0$ (lower face of shock plate) is $\bar{T}(0,s)$, which can be substituted in Eq. 17 to determine A_1:

$$A_1 = \frac{\bar{T}(0,s)}{e^0} = \bar{T}(0,s). \tag{18}$$

Substituting this value of A_1 in Eq. 17 yields

$$\bar{T}(x,s) = \bar{T}(0,s)\ e^{-x\sqrt{s/K}}\ , \text{ or}$$

$$\frac{\bar{T}(x,s)}{\bar{T}(0,s)} = e^{-x\sqrt{s/K}}\ . \tag{19}$$

When the initial temperature at x = 0, which is represented by $\bar{T}(0,s)$, is replaced by a unit step function, $U(\theta) = \frac{1}{s}$, to simulate a step change in temperature, Eq. 19 becomes

$$\bar{T}(x,s) = \frac{1}{s}\, e^{-x\sqrt{s/K}}. \tag{20}$$

To obtain the response in the time domain, Eq. 20 must first be inverted. From the table of Laplace transforms,

$$L^{-1}\left[\frac{1}{s}\, e^{-x\sqrt{s/K}}\right] = \frac{2}{\sqrt{\pi}} \int_{x}^{\infty} e^{-x^2/4K\theta}\, dx. \tag{21}$$

The right side of this equation is the error-function complement of x, which is defined as

$$\text{erfc } x = 1 - \frac{2}{\sqrt{\pi}} \int_{0}^{x} e^{-U^2}\, dU$$

$$= \frac{2}{\sqrt{\pi}} \int_{0}^{\infty} e^{-U^2}\, dU. \tag{22}$$

Using the transform pair given in Eq. 21, Eq. 20 becomes

$$\bar{T}\ (x,\theta) = \text{erfc}\ \frac{x}{\sqrt{4K\theta}}\ . \tag{23}$$

When determining the temperature variation with time at any surface ℓ ft from x = 0, Eq. 23 is written

$$T(\ell,\theta) = \text{erfc}\ \frac{\ell}{\sqrt{4K\theta}}\ , \qquad (24)$$

where $T(\ell,\theta)$ = drop in temperature, in °F, at $x = \ell$ and at time θ.

Equation 24 was used to calculate the drops in temperature with time θ at the lower face (ℓ = 0.0625 ft) and upper face (ℓ = 0.3125 ft) of the tubesheet as a result of the scram-induced step change of 150°F at the lower face of the shock plate. Table X lists the calculated temperature drops (ΔT_L) at ℓ = 0.0625 ft and Table XI the calculated drops (ΔT_U) at ℓ = 0.3125 ft.

Figure 14 plots these temperature drops, and the difference between them, with respect to time. The difference between ΔT_U and ΔT_L reaches a maximum of 97°F approximately 250 sec after the step change in temperature. The thermal stress in the tubesheet that results from this temperature difference is calculated from Eq. 6,

$$\sigma_t = \frac{E\alpha\Delta T}{2(1-\nu)}\ ,$$

where

σ_t = thermal stress, in psi;

E = modulus of elasticity, in psi (=23.1 x 10^6 @ 800°F);

α = instantaneous value of the coefficient of thermal expansion, in in./in.-°F. (=11 x 10^{-6} at 800°F);

ν = Poisson's ratio (=0.3); and

$\Delta T = \Delta T_U - \Delta T_L$ = 97°F.

By substitution,

$$\sigma_t = \frac{(23.1 \times 10^6)(11 \times 10^{-6})}{2\,(1 - 0.3)}\,97$$

$$= (181.5)(97)$$

$$= 17{,}600 \text{ psi.}$$

TABLE X. Temperature Drop (ΔT_B) with Respect to Time (θ) at Lower Face of Upper Tubesheet of IHX after Sudden 150°F Drop in Temperature at Lower Face of Shock Plate

Time (θ), sec	$\frac{0.0625}{\sqrt{4K\theta}}$	$\text{erfc}\frac{0.0625}{\sqrt{4K\theta}}$	Temperature Drop (ΔT_I), °F
1	4.2[illegible]	0.00002	0.00
5	1.91[illegible]	0.00641	0.96
6	1.748	0.00815	1.22
7	1.619	0.02224	3.34
8	1.514	0.03246	4.87
9	1.428	04385	6.58
10	1.354	0.05612	8.42
20	0.958	0.17572	26.36
30	0.782	0.26904	40.36
40	0.677	0.33865	50.80
50	0.606	0.39156	58.73
100	0.428	0.54524	81.79
200	0.303	0.66823	100.24
300	0.247	0.72046	108.07
400	0.214	0.76228	114.34
500	0.192	0.78605	117.91
600	0.175	0.80465	120.70
800	0.151	0.83091	124.64
1000	0.135	0.84866	127.30
2000	0.096	0.88305	132.46

TABLE XI. Temperature Drop (ΔT_U) with Respect to Time (θ) at Upper Face of Upper Tubesheet of HX after a Sudden 150°F Drop in Temperature at Lower Face of Shock Plate

Time (θ), sec	$\frac{0.3125}{\sqrt{4K\theta}}$	erfc $\frac{0.3125}{\sqrt{4K\theta}}$	Temperature Drop (ΔT_U), °F
1	21.414	0	0
5	9.557	0	0
10	6.772	0	0
20	4.778	0	0
30	3.910	0	0
40	3.386	0	0
50	3.028	0	0
100	2.141	0.00252	0.38
200	1.514	0.03246	4.87
300	1.236	0.08368	12.55
400	1.071	0.13067	19.60
500	0.958	0.17572	26.36
600	0.874	0.21674	32.51
800	0.757	0.28451	42.68
1000	0.677	0.33865	50.80
2000	0.479	0.49841	74.76

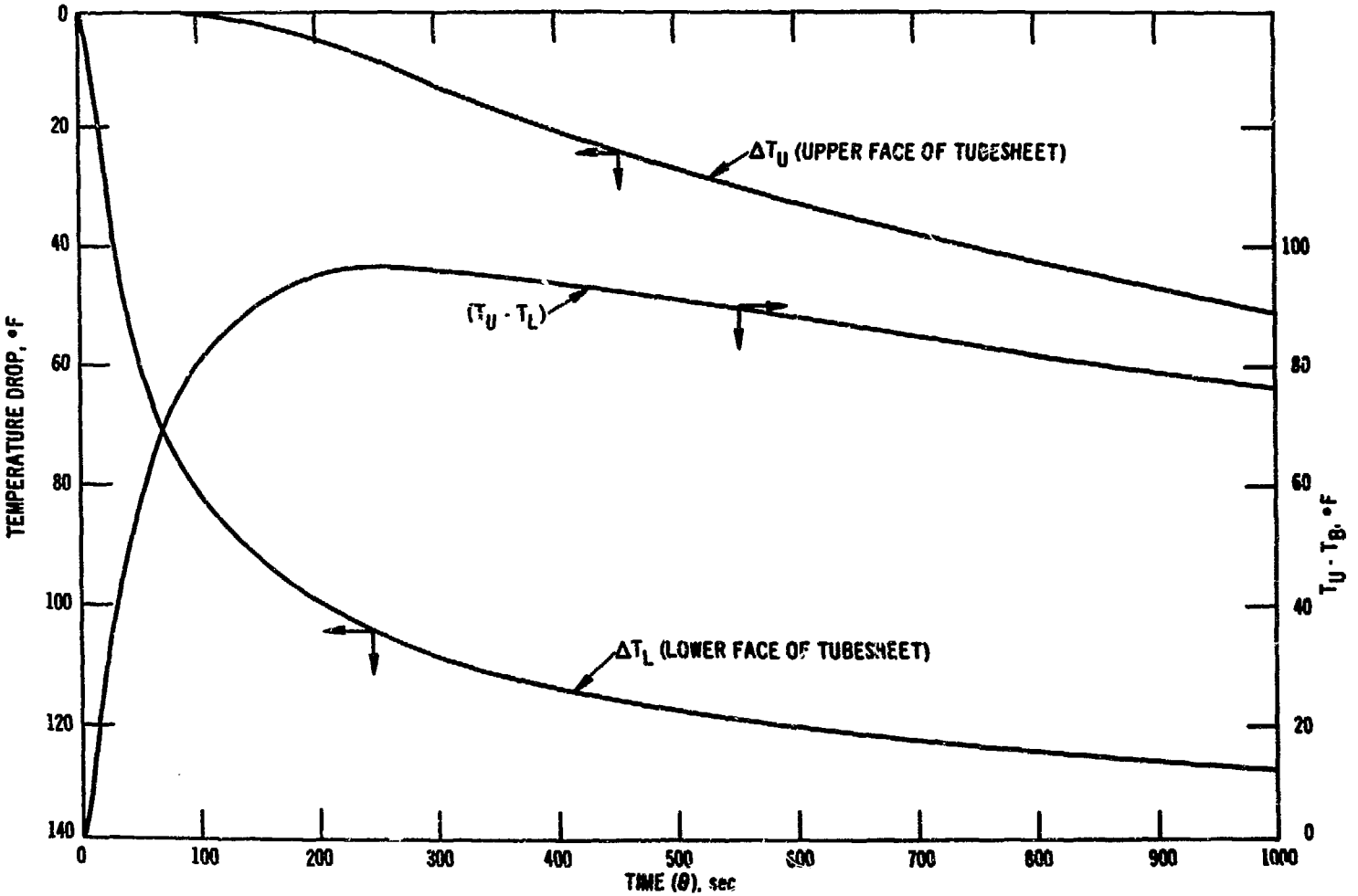

Fig. 14. Temperature Transients in Upper Tubesheet of IHX after Reactor Scram

APPENDIX B

Steady-state Thermal Stresses in the Well Casing of the Intermediate Heat Exchanger

Temperatures detected by thermocouples RI-TC-507-DR and RI-TC-501-S in the well casing (U nozzle) of the EBR-II intermediate heat exchanger (IHX) indicate that hot (883°F) primary sodium is forced upward in the annulus between the well casing and the tube-bundle structure during steady-state operation. This upward thrust of hot sodium in the annulus is believed to cause relatively high stresses in the 3/4-in. circumferential fillet weld by which the well casing is attached to the bottom plate of the reactor-tank cover. This appendix uses a simplified method to calculate the steady-state stresses in this weld.

Figure 15 shows the location of the weld, and gives dimensions and materials of construction pertinent to the calculations. Figure 16 is a free-body diagram of the cross section of the weld. (The symbols not defined in the figures are defined in the text following.) The average temperature of the bottom plate near the weld is 600°F, and that of the well casing near the weld is 880°F.

The following assumptions were made in making the calculations:

1. The opening for the well casing in the bottom plate retains its size corresponding to a 600°F mean temperature of the plate.

2. The deformation of the well casing is caused by the temperature difference of 280°F (880-600°F) between the well casing and the bottom plate.

3. The circumferential reaction to counteract the force caused by differential radial expansion is furnished by the fillet weld.

The deflection (δ) of a long, cylindrical shell by an elementary ring load of an intensity $q\,d\xi$ is given by [5]

$$\delta = \frac{qa^2}{2Eh}\left(2 - e^{-\beta b}\cos\beta b - e^{-\beta c}\cos\beta c\right), \qquad (25)$$

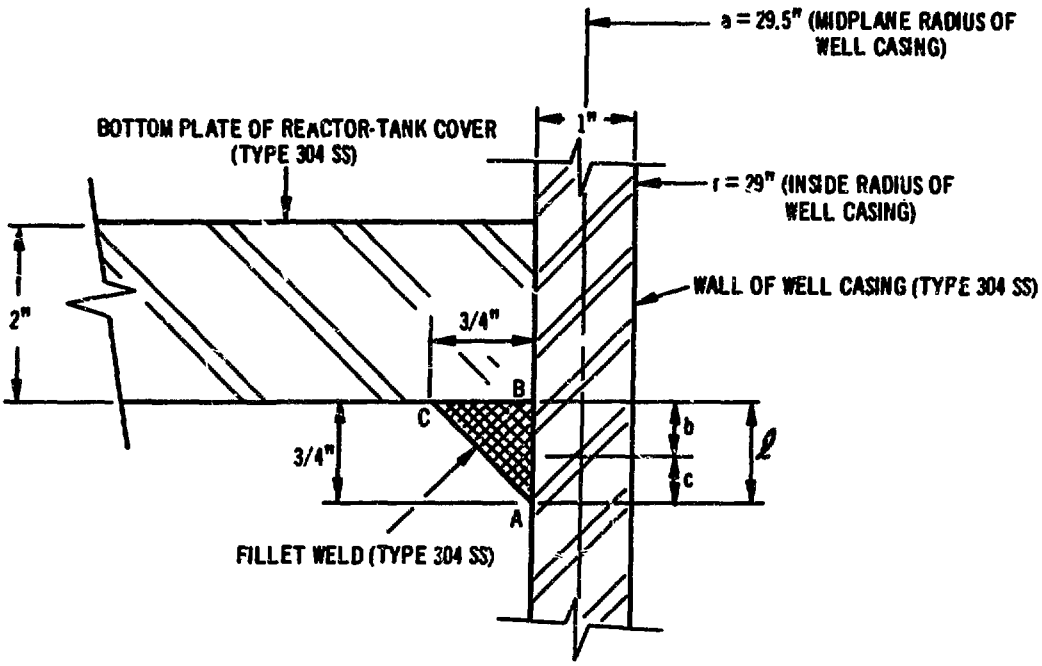

Fig. 15. Location of Fillet Weld Holding IHX Well Casing to Bottom Plate of Reactor-tank Cover

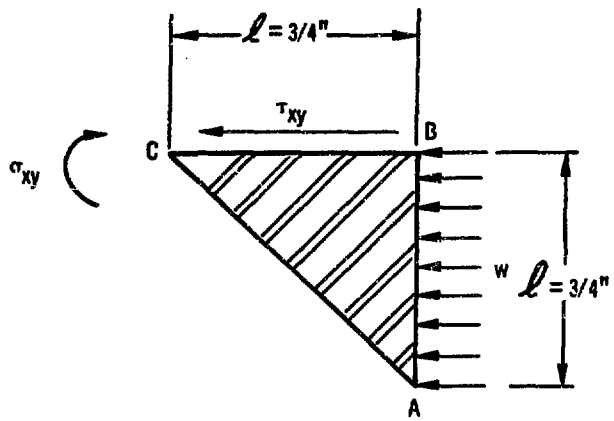

Fig. 16. Free-body Diagram of Cross Section of Well-casing Fillet Weld

where

δ = radial deflection, in in.;

q = uniformly distributed load, in psi;

a = midplane radius of shell, in in. (=29.5);

E = modulus of elasticity, in psi (=22 x 10^6 @ 900°F);

h = shell thickness, in in. (=1);

b = distance from point at which stress is being determined to point B, in in.;

c = distance of the same point of stress from point A, in in.; and

$$\beta = \sqrt[4]{\frac{3(1 - \nu^2)}{a^2h^2}}, \text{ in in.}^{-1}, \tag{26}$$

where

ν = Poisson's ratio (=0.3).

The radial deflection of the shell (the IHX well casing) caused by thermal expansion of the casing will impose a uniformly distributed load on the "belt" that extends from point A to point B. The amount of this deflection (δ) is calculated from the equation

$$\delta = \alpha \Delta T (r + h), \tag{27}$$

where

α = linear coefficient of thermal expansion, in in./in.-°F (= 10 x 10^{-6});

ΔT = temperature difference causing the expansion, in °F (=280); and

r = inside radius of shell, in in. (=29).

Substitution of the numerical values in Eq. 27 gives

$$\delta = (10 \times 10^{-6})(280)(29 \div 1)$$

$$= 0.084 \text{ in.}$$

Substituting this value of δ in Eq. 25 and solving for q, we obtain

$$q = (0.168(\frac{Eh}{a^2})(2 - e^{-\beta b}\cos\beta b - e^{-\beta c}\cos\beta c)^{-1}. \quad (28)$$

Since the stress will be greatest at the edges of the belt, (points A and B), Eq. 28 can be simplified for calculating the stress at one of thos points.

At point A, b = 0.75 and c = 0 (see Fig. 15). Thus, Eq. 28 becomes

$$q = \frac{0.168\ Eh}{a^2(1 - e^{-\beta b}\cos\beta b)}. \quad (29)$$

β can be determined from Eq. 26:

$$\beta = \sqrt[4]{\frac{3[1 - (0.3)^2]}{(29.5)^2(1)^2}} = 0.237 \text{ in.}^{-1}.$$

Substituting the numerical value in Eq. 29, we obtain

$$q = \frac{(0.168)(22 \times 10^6)(1)}{(29.5)^2(1 - e^{-0.1775}\cos\ 0.1775)}$$

$$= \frac{3.696 \times 10^6}{870.25(0.1758)}$$

$$\approx 24{,}200 \text{ psi.}$$

The maximum shear stress, τ_{xy}, is the same as q (≈24,200 psi).

Bending stress at point C can be calculated as follows:

$$\sigma_{xy} = k \frac{M_{xy}}{S_M}, \tag{30}$$

where

σ_{xy} = bending stress, in psi;

k = stress-intensification factor (=2*);

M_{xy} = bending moment, in in.-lb;

S_M = section modulus of the area whose length (ℓ) is $\overline{BC}$ and width is 1 in. [$= \frac{1}{6}(1)(\ell)^2 = \frac{1}{6}(\frac{3}{4})^2 = 0.09375$ in.^{3}].

When the weld is treated as a cantilever beam with a uniform load of w lb/in., the bending moment at point C is given by

$$M_{xy} = -\frac{1}{2} w\ell^2, \tag{31}$$

where w = uniformly distributed load, in lb/in. (=q=24,200 for a unit segment of the weld circumference); and

ℓ = 3/4 in.

By substitution in Eq. 31, we obtain

$$M_{xy} = -(\tfrac{1}{2})(24{,}200)(\tfrac{3}{4})^2$$

$$= -6806 \text{ in.-lb.}$$

*Assumed value. Plastic deformation after the first stress cycle will make this coefficient smaller.

So, from Eq. 30,

$$\sigma_{xy} = -2 \left(\frac{6806}{0.09375}\right)$$

$$= -(2)(72,600)$$

$$= -145,200 \text{ psi.}$$

Principal stress, S_1, can be determined from

$$S_1 = \frac{1}{2}\sigma_{xy} \pm \sqrt{\left(\frac{1}{2}\sigma_{xy}\right)^2 + (\tau_{xy})^2} \,. \tag{32}$$

Substitution of the numerical values gives

$$S_1 = \frac{1}{2}(145,200) - \sqrt{\left(\frac{145,200}{2}\right)^2 + (24,200)^2}$$

$$= -72,600 - 76,530$$

$$= -149,130 \text{ psi.}$$

If S_1 is considered as a stress range, its amplitude will be

$$S_a' = \frac{1}{2}S_1$$

$$= 74,570 \text{ psi.}$$

Figure 5 shows that, at this amplitude and at the temperature of point C (~830°F), the number of cycles to fatigue is approximately 2000.

ACKNOWLEDGMENTS

The author gratefully acknowledges contributions from various personnel of ANL. In particular, he thanks: L. K. Chang and J. F. Koenig for their technical review of the manuscript; H. O. Monson for briefing the author on the design philosophy and criteria of the reactor vessel, IHX,and primary-sodium piping; R. W. Seidensticker for consultation on the reactor tank and the IHX well casing; G. S. Rosenberg and P.Y. Wang for their consultation on evaluating some thermal stresses in the IHX well casing; C. C. Stone for furnishing predicted temperature gradients in the steam generators; and M. Shackelford for his suggestions on devising Figs. 10 and 12.

REFERENCES

1. ASME Boiler and Pressure Vessel Code, The American Society of Mechanical Engineers, New York.

2. R. A. Cushman et al., Operation of EBR-II at 62.5 MWt: An Evaluation of Plant and Reactor Data from Run 38A, ANL/EBR-013 (to be published).

3. L. J. Koch et al., Hazard Summary Report, Experimental Breeder Reactor II (EBR-II), ANL-5719 (May 1957).

4. L. J. Koch, W. B. Loewenstein, and H. O. Monson, Addendum to Hazard Summary Report, Experimental Breeder Reactor II (EBR-II), ANL-5719 (Addendum) (June 1962).

5. S. Timoshenko and S. Woinowsky-Krieger, Theory of Plates and Shells, 2nd Ed., pp. 474-475, McGraw-Hill, New York (1959).